Optics Letters

Engineering of energy band and its impact on the light transmission in a non-reciprocal Hermitian hourglass lattice

Junhao Yang, Yuandan Wang, Yu Lin, Wenjing Zhang, Guoguo Xin, and Xinyuan Qi*

School of Physics, Northwest University, Xi'an 710127, China
**qixycn@nwu.edu.cn*

Received 28 November 2023; revised 11 December 2023; accepted 11 December 2023; posted 11 December 2023; published 1 January 2024

We study a quasi-one-dimensional non-reciprocal Hermitian hourglass photonic lattice that can accomplish multiple functions. Under the effect of non-reciprocal coupling, this lattice can produce an energy isolation effect, two kinds of flatbands, and energy band inversion. The excitation and propagation of a single energy band and multiple energy bands can be realized; in the flatband condition, the system has compact localized states, and the flatbands can be excited by a straightforward method. Our findings advance the theory of energy band regulation in artificial photonic lattices.

https://doi.org/10.1364/OL.514572

Discrete transmission of optical waves, as one of the essential means of spatial optical modulation, is mainly realized by the joint action of trapping in weak waveguides and evanescent coupling between near-adjacent waveguides [1]. In recent years, most discrete optical transmission research uses periodic photonic lattices as the research platform. Photonic lattice, a renowned physical model with periodically modulated refractive index change in space, is widely used to explore the light dynamics in discrete optical systems, one of the essential platforms for various optical research [2,3]. In such lattices, the coupling between the adjacent waveguides is symmetrical, and the energy transfer is reversible. Thus, these lattices are called reciprocal coupling photonic lattices, and the same coupling coefficient between the lattice sites characterizes their structures. Furthermore, some photonic phenomena can be observed through evanescent couplings, such as discrete diffraction [4], optical Bloch oscillations [5], dynamic localization [6], and Zener tunneling [7]. In reality, the shape of a single waveguide can be asymmetric about its transmission axis. That is due to fabrication process limitations or for some particular purposes. As a result, the coupling effect between the near-adjacent waveguides is non-reciprocal. Hence, a non-reciprocal coupling photonic lattice is formed [8,9]. Besides, the replacement of straight waveguides with staggered helical ones in photonic lattices will result in an additional asymmetric phase factor $e^{\pm i\varphi}$ in the coupling coefficient, which is also another way to obtain a non-reciprocal coupling photonic lattice [10–12].

Once the intrinsic coupling coefficients of waveguides and the lattice geometry are chosen, the energy band structure is determined, ultimately affecting how light behaves in the lattice. Therefore, designing the band structure is one of the most critical methods to regulate the light transmission [13,14]. Since lattice geometry is usually not easily changeable, the lattice intrinsic coupling coefficient naturally becomes the preferred variable for regulating energy bands [15]. Many intriguing phenomena have emerged because of this, such as topological property [3], bandgap and touch [16,17], adjustable flatband [18], and band inversion [19].

Flatbands [20–24], a type of special energy band structures in condensed physics and photonics, are well known for their zero dispersion in at least one energy band of their spectra. Various flatband lattices have been theoretically and experimentally constructed, such as one-dimensional flatband lattices [22], Lieb lattices [23], and Kagome lattices [24] and the square-root topological rhombic lattice [25]. The most typical common feature of these systems is that their eigenmodes are localized in real space; namely, they all support the existence of compact localized states (CLS) [20–24]. Although various intriguing phenomena have been inspired by the flatband features, such as topological superconductor [26], topological flatband insulator [27], and Anderson localization [28]. Most of these studies are performed in reciprocal systems; meanwhile, one structure achieves only a single function. So, realizing flatbands and multifunctional systems in a non-reciprocal system is still an interesting challenge.

In this work, we propose a quasi-one-dimensional non-reciprocal Hermitian hourglass photonic lattice. We find that the Peierls phase term of the non-reciprocal coupling coefficient influences the system's energy band structure and the light energy distribution. By tuning the Peierls phase, we can obtain different energy bands, such as flatband, band inversion, and stable band, which are insensitive to the Peierls phase. We calculate the light energy distribution and observe the energy isolation effect induced by the Peierls phase. We also use Gaussian beams to excite the lattice to confirm the theoretical predictions. Moreover, we show that different excitation conditions can lead to single or double-band excitation. We investigate the CLSs of the flatband and use a novel method to excite the flatband.

We first construct an hourglass photonic lattice model that consists of three sites (A_n, B_n, and C_n) per unit cell, as shown in Fig. 1, where n is the lattice site number, κ_1 is the intracell coupling coefficient, κ_2 is the intralayer coupling coefficient, and

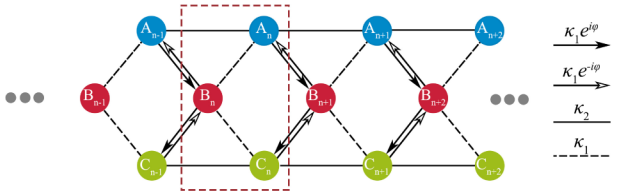

Fig. 1. Schematic of the hourglass photonic lattice. The arrows represent the non-reciprocal couplings and photon tunneling direction. The carmine-dashed box represents a unit cell.

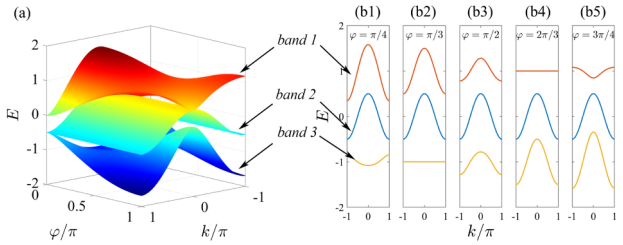

Fig. 2. Energy band structures. (a) Surface of bands versus the wave vector k and Peierls phase φ. (b1)-(b5) The energy band curves under different φ. Here, $\kappa_1 = 0.5$, $\kappa_2 = 0.25$.

$\kappa_1 e^{\pm i\varphi}$ is the intercell coupling coefficient; φ is the non-reciprocal coupling phase, also known as the Peierls phase, whose positive or negative sign depends on the direction of photon tunneling.

Under periodic boundary conditions, the Hamiltonian of this model in momentum space is given by

$$\boldsymbol{H} = \begin{pmatrix} 2\kappa_2 \cos k & \kappa_1 + \kappa_1 e^{i(k-\varphi)} & 0 \\ \kappa_1 + \kappa_1 e^{i(\varphi-k)} & 0 & \kappa_1 + \kappa_1 e^{-i(k+\varphi)} \\ 0 & \kappa_1 + \kappa_1 e^{i(k+\varphi)} & 2\kappa_2 \cos k \end{pmatrix}, \quad (1)$$

where k is the Bloch wave vector in the first Brillouin zone (Hamiltonian in real space, see Supplement 1). By analyzing the Bloch Hamiltonian, we find that it satisfies $\boldsymbol{H} = \boldsymbol{H}^{\dagger}$ despite the existence of a non-reciprocal coupling coefficient in the lattice, meaning that the system is a Hermitian one with real energy spectra. Solving the Hamiltonian $\boldsymbol{H}$, we can obtain the expression of the band structures as follows:

$$E_{2,1/3}(k,\varphi) = 2\kappa_2 \cos k, \kappa_2 \cos k \pm \frac{\sqrt{2}}{2}\sqrt{8\kappa_1^2 + \kappa_2^2 + \kappa_2^2 \cos 2k + 8\kappa_1^2 \cos k \cos \varphi}. \quad (2)$$

According to Eq. (2), we obtain the energy band structure of the system as shown in Fig. 2. From Fig. 2(a), we can see that the energy band 2 is stable, while bands 1 and 3 vary with the change of Peierls phase φ. The inversion for band 1 is realized by increasing the Peierls phase from $\varphi = \pi/4$ to $\varphi = 3\pi/4$ [see the orange curves in Figs. 2(b1)-(b5)]; similar phenomenon happens with band 3 [see the yellow curves in Figs. 2(b1)-(b5)]. Besides, when the Peierls phase φ is $\pi/3$ or $2\pi/3$, flatbands appear in the energy band structure, as shown in Figs. 2(b2, b4), indicating that the CLSs could exist under these two conditions. Further studying the group velocity v_g ($v_g = \partial E/\partial k$, see Supplement 1 for specific formula and figures), the diffraction-free transmission will be obtained at $(k,\varphi) = (\pm\pi/2, \pi/3)$ or $(k,\varphi) = (\pm\pi/2, 2\pi/3)$ since the first derivative of v_g is zero.

Based on the above analysis, we conclude that the Peierls phase φ governs most of the physical phenomena in the system. Therefore, we theoretically study the impacts of Peierls phase φ on the eigenstates of the system with stationary solution method [29]. Firstly, we substitute the stationary solution $(a_n, b_n, c_n)^T = \exp(-i\Lambda z)(\mathrm{A}_n, \mathrm{B}_n, \mathrm{C}_n)^T$ into Eq. (1), and obtain the static equation,

$$\Lambda\zeta_n = \boldsymbol{H}\zeta_n, \quad (3)$$

where Λ is the stationary frequency, $\zeta_n = (a_n, b_n, c_n)^T$ and the corresponding $(\mathrm{A}_n, \mathrm{B}_n, \mathrm{C}_n)^T$ describes the z-independent amplitudes at the nth waveguide in layers A, B, and C, respectively. Secondly, to simplify the operation, $(\mathrm{A}_n, \mathrm{B}_n, \mathrm{C}_n)^T$ is expressed as $(\mathrm{A}_n, \mathrm{B}_n, \mathrm{C}_n)^T = \{\exp[-i(kn + \delta_a)], \exp[-i(kn + \delta_b)], \exp[-i(kn + \delta_c)]\}(a, b, c)^T$, where δ_a, δ_b and δ_c are the initial phase and set to be zero for simplification and $(a, b, c)^T$ is n-independent amplitudes in layers A, B, and C. Finally, substituting the assumed solution into Eq. (3) (see Supplement 1 for specific formula) and considering the energy conservation of the system, $|\mathrm{A}_n|^2 + |\mathrm{B}_n|^2 + |\mathrm{C}_n|^2 = 1$, we obtain the energy distributions:

$$|\mathrm{A}_n|^2 = \frac{2\kappa_1^2[1 + \cos(k + \varphi)]}{f(k,\varphi)}, \quad (4)$$

$$|\mathrm{B}_n|^2 = \frac{[\Lambda - 2\kappa_2 \cos k]^2}{f(k,\varphi)}, \quad (5)$$

$$|\mathrm{C}_n|^2 = \frac{2\kappa_1^2[1 + \cos(k - \varphi)]}{f(k,\varphi)}, \quad (6)$$

where Eqs. (4)–(6) hold when $f(k,\varphi) = 4\kappa_1^2 + 2\kappa_2^2 + \Lambda^2 + 2\kappa_2^2 \cos 2k + 4\cos k[\kappa_1^2 \cos\varphi - \kappa_2\Lambda] > 0$. We set $\kappa_1 = 0.5$, $\kappa_2 = 0.25$, $\Lambda = 1.5$, $k \in [-\pi, \pi]$, $\varphi \in [0, \pi]$ and verify that $f(k,\varphi) > 0$ holds for all values of k and φ.

According to Eqs. (4)–(6), the light energy distribution maps in three layers with respect to the wave vector k and the Peierls phase φ are obtained as shown in Figs. 3(a1–a3). When $k = \pm\pi/2$ and $\varphi \in [\pi/5, 4\pi/5]$ (see lines l_1 and l_2), the vast majority of the light energy appears in layers A and B or layers B and C [Figs. 3(a1–a3)]; apparently, these lead to the energy isolation of layer C or layer A, respectively. Further, considering the solutions are stationary, the energy in these three layers will remain invariant once a plane wave is incident at point P(k, φ) on lines l_1 or l_2.

To verify the above conclusions, we numerically simulate the evolution of three Gaussian beams with intensity functions:

$$I = U_A e^{-(\frac{n_A - n_{A0}}{\omega})^2 + ik_0 n_A} + U_B e^{-(\frac{n_B - n_{B0}}{\omega})^2 + ik_0 n_B} + U_C e^{-(\frac{n_C - n_{C0}}{\omega})^2 + ik_0 n_C}, \quad (7)$$

where $U_{(A,B,C)}$ are the amplitudes, satisfying $U_A/U_B/U_C = I_A(k,\varphi)/I_B(k,\varphi)/I_C(k,\varphi)$, $I_{(A,B,C)}$ are the intensities at points P_A, P_B and P_C in Figs. 3(a1-a3); $n_{(A,B,C)0}$ are the incident lattice site numbers, ω is the width of the Gaussian beam and k_0 is the initial wave vector. When $I_{(A,B,C)}$ are at points $P_{(A,B,C)}$ with wave vector $k_0 = -\pi/2$ [see Figs. 3(b1–b3)], most of the energy distributes in layers A and B, while the layer C is isolated; When $I_{(A,B,C)}$ are at points $P_{(A',B',C')}$ with wave vector $k_0 = \pi/2$ [see Figs. 3(c1–c3)], most of the energy distributes in layers B and C, while the layer A is cut off. Besides, the intensity distribution in each layer depends on the value of Peierls phase φ. When $\varphi = \pi/4$ or $2\pi/3$, light bifurcates into two sidelobes, respectively [see Figs. 3(b1, b2) and 3(c1, c2)]; In particular, for $\varphi = \pi/2$, oscillating localizations of light beams are supported between lattice layers A and

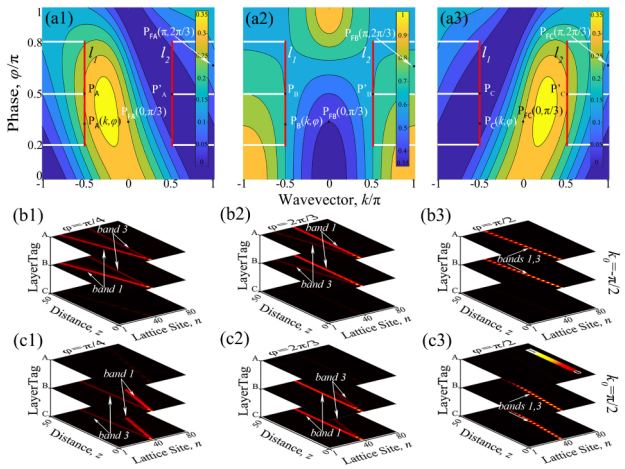

Fig. 3. Characterization of light transmission. (a1)–(a3) Maps of light energy distributions of layers A, B, and C versus the Peierls phase φ and the wave vector k. (b1)–(b3) and (c1)–(c3) Numerically calculated light evolution (Two other conditions: $\varphi = \pi/3$ and $3\pi/4$ are shown in Supplement 1 for specific figures). Here, Λ=1.5, $\kappa_1 = 0.5$, $\kappa_2 = 0.25$.

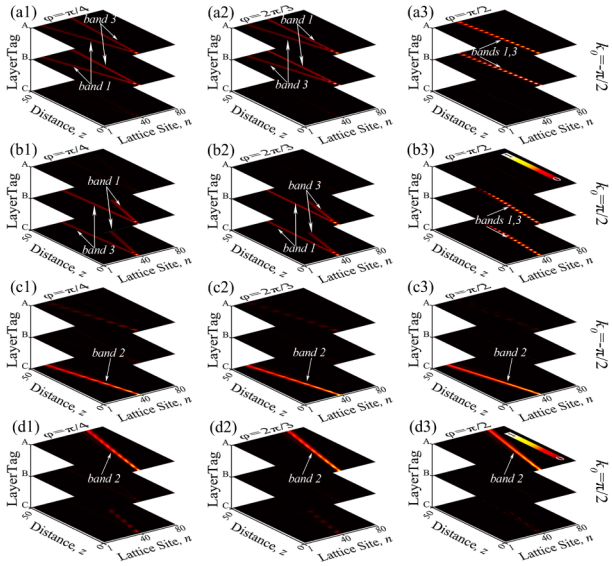

Fig. 4. Simulations of single and double energy bands excitations. (a1)–(a3) and (b1)–(b3) Excitation at $k = \mp\pi/2$ in layer B with different φ. (c1)–(c3) and (d1)–(d3) Excitation at $k = \mp\pi/2$ in layer C and A with different φ (Two other conditions: $\varphi = \pi/3$ and $3\pi/4$ are shown in Supplement 1 for specific figures). Here, $\kappa_1 = 0.5$, $\kappa_2 = 0.25$, $\omega = 2$.

B with incident wave vector $k_0 = -\pi/2$ or B and C with incident wave vector $k_0 = \pi/2$, both propagating along one direction [see Figs. 3(b3, c3)]. It should be noted that the ratios among the three layers are slightly deviated from the theoretical values calculated by Eqs. (5) and (6), which can be attributed to the use of the Gaussian beams instead of plane waves. Notably, all these propagations are along the perpendicular directions of the tangent of bands 1 and 3. Moreover, two sidelobes in Figs. 3(b1, b2) and 3(c1, c2) exchange their energy band numbers due to the band inversion, which is consistent with the results in Figs. 2(b1, b4). These results indicate that the energy band excitation and engineering could be achieved by tuning the parameters of k_0 and φ.

We further investigates the light transmission properties resulting from a single Gaussian beam incident in the lattice. Figures 4(a1–a3) and (b1–b3) illustrate the light wave evolution results when a single Gaussian beam is injected in layer B. We refer to this incident beam as a nearly steady state beam, which satisfies $U_A/U_B/U_C = 0/1/0$. From Figs. 4(a1–a3) and (b1–b3), energy isolation appears: most energy distributes in layers A and B at $k_0 = -\pi/2$ or layers B and C at $k_0 = \pi/2$. Besides, all transmissions result from the excitation of energy bands 1 and 3. Also, the switch of energy band numbers between two sidelobes due to band inversion exists [see Figs. 4(a1, a2) and 4(b1, b2)]. Additionally, the propagations of the special case that $\varphi = \pi/2$ are still oscillatory and localized [see Figs. 4 (a3, b3)]. These results are all consistent with the above conclusion using a steady state beam. However, one difference is that the energy in sidelobes is no longer mostly concentrated on the excited sidelobe of band 1, and the energy in the excited sidelobe of band 3 has become comparable to that of band 1 [see Figs. 3(b1, b2, c1, c2) and Figs. 4 (a1, a2, b1, b2)]. In addition, the excitation of double energy bands involves flatbands [see Figs. 3(b2, c2) and Figs. 4(a2, b2)]. Because the flatband exists when $\varphi = 2\pi/3$ [see Fig. 2(b4)], and are located in band 1.

When a single Gaussian beam is input in layer C or A at $k_0 = -\pi/2$ and $k_0 = \pi/2$, respectively, light energy is almost confined in the incident layer C or A due to the energy isolation as shown in Figs. 4(c1–c3, d1–d3). The incident beam is called away steady state beam, which has $U_A/U_B/U_C = 0/0/1$ at $k_0 = -\pi/2$ and $U_A/U_B/U_C = 1/0/0$ at $k_0 = \pi/2$. In contrast to incident steady or nearly steady beam, the propagation does not bifurcate. Also, all lights propagate along the perpendicular direction of the tangent of the stable band 2. Based on the analyses above, the excitation conditions depend not only on the wave vector k and Peierls phase φ but also on the initial incident site. Therefore, we can determine a particular excitation band by specifying the values of φ, k, and the incident position.

In the analysis above, we have realized the excitation of the mixed energy band, in which the other curve band still influences the flatband excitation. The CLS mode excitation with multibeam incidence has been studied theoretically and experimentally [22,23]. However, the study on flatband excitation with a single beam still needs to be explored. Considering the simple optical path configuration and potential applications in light manipulation, a single beam excitation might be more meaningful, although the physical mechanism is still unclear.

In Figs. 2(b2, b4), the hourglass lattice has two kinds of flatbands. For $\kappa_1 = 0.5$, $\kappa_2 = 0.25$ and $\varphi = \pi/3$, the flatband energy is $E_{FB} = -1$. When $\varphi = 2\pi/3$, the flatband energy is $E_{FB} = +1$. We apply the fundamentals to excite the flatband first and calculate the distribution of wave function amplitudes at different lattice sites, which can be efficiently evaluated using a Schrödinger equation of the form:

$$(E - \epsilon_i)\psi_i = \sum_j \kappa_{ij}\psi_j, \tag{8}$$

where ϵ_i is the on-site potential at the ith site, κ_{ij} is the coupling amplitude between neighboring sites, and ψ_i is the wave function amplitude at the ith site. Figures 5(a, b) illustrate the wave function amplitude distribution corresponding to the CLSs with energies $E_{FB} = -1$ and $E_{FB} = +1$. The wave function corresponding to the CLSs is localized over a finite number of

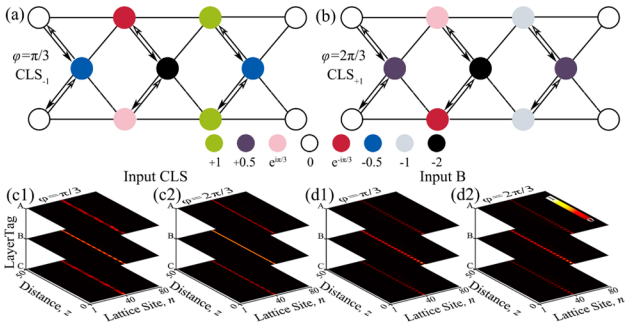

Fig. 5. Compact localized states (CLS) and flatband excitation. (a), (b) CLS mode for $E = -1$ and $E = 1$, respectively. The colors represent the filled amplitude. (c1), (c2) Excitations with CLS_{-1} and CLS_{+1} modes at $k_0 = \pi$ when $\omega = 1$. (d1), (d2) Excitation with a single Gaussian beam from layer B at $(k_0, \varphi) = (0, \pi/3)$ and $(k_0, \varphi) = (\pi, 2\pi/3)$, respectively, when $\omega = 2$. Here, $\kappa_1 = 0.5$, $\kappa_2 = 0.25$.

lattice sites with non-zero amplitudes (marked by solid-colored circles). Beyond those sites, the amplitude of the wave function is zero (marked by open circles).

Figures 5(c1, c2) show the numerical simulation of light propagation by inputting Gaussian beam arrays, which constitute CLS modes. All the light beams propagate straightly and locally in layers A, B, and C, and the energy primarily concentrates in layer B, demonstrating that the CLS modes in Figs. 5(a, b) are the flatband modes exactly. Though this method successfully excites a single flatband, it is complex.

In the following, we further study the operation principle of a single flatband excitation with a single beam incidence. We employ a single Gaussian beam to excite a single flatband. We inject the beam with normal incidence ($k_0 = 0$) into layer B with $\varphi = \pi/3$. As seen in Fig. 5(d1), light propagates straightly and locally in three layers, showing that a simple excitation method is practicable. Similarly, light also achieves the diffraction-free oscillating localization among the three layers when a Gaussian beam with wave vector $k_0 = \pi$ is incident into layer B with $\varphi = 2\pi/3$ [Fig. 5(d2)]. Besides, most of the light energy in Figs. 5(d1, d2) is in layer B, and the rest is equally distributed in layers A and C. The reason for these phenomena can be found in Figs. 3(a1-a3), the intensities in waveguides A_n, B_n, and C_n satisfying $|A_n|^2 = |C_n|^2 < |B_n|^2$ at $k = 0, \pi$ when $\varphi = \pi/3, 2\pi/3$, respectively [attention to the intensity value represented by the color in points $P_{FA(B,C)}(0, \pi/3)$ and $P_{FA(B,C)}(\pi, 2\pi/3)$]. In addition, the oscillating localization among the three layers can only be caused by the single flatband excitation since the group velocity dispersions for the other two bands are non-zeroes. Our method provides a simple way to achieve individual flatband excitation and provides a novel perspective on energy band manipulation. Based on the above conclusions, an applicable experimental project is given in the Supplement 1.

In conclusion, We have investigated a quasi-one-dimensional non-reciprocal Hermitian hourglass photonic lattice in which energy bands are tunable by changing the non-reciprocal coupling coefficient φ. The lattice can realize energy band inversion and flatbands as φ changes. By calculating the interlayer distribution of light energy, we found that the system has an energy isolation effect: layers A and B are isolated from layer C when $k = -\pi/2$, or layers B and C are isolated from layer A when $k = \pi/2$. Subsequently, during the verification process, we can determine the specific excitation band once we confirm the values of φ, k, and the incident position. In flatband excitation, we can use CLSs to excite flatbands and a more straightforward single beam to excite flatbands. Our research results may provide opportunities to explore new theories of energy band regulation in artificial photonic lattices.

Funding. National Natural Science Foundation of China (12174307).

Disclosures. The author declares no conflicts of interest.

Data availability. No data were generated or analyzed in the presented research.

Supplemental document. See Supplement 1 for supporting content.

REFERENCES

1. F. Lederer, G. I. Stegeman, D. N. Christodoulides, *et al.*, Phys. Rep. **463**, 1 (2008).
2. J. W. Fleischer, M. Segev, N. K. Efremidis, *et al.*, Nature **422**, 147 (2003).
3. Z. Lan, M. L. Chen, F. Gao, *et al.*, Rev. Phys. **9**, 100076 (2022).
4. T. Pertsch, U. Peschel, F. Lederer, *et al.*, Opt. Lett. **29**, 468 (2004).
5. T. Pertsch, P. Dannberg, W. Elflein, *et al.*, Phys. Rev. Lett. **83**, 4752 (1999).
6. Y. Deng, J. Lin, Z. Sun, *et al.*, Phys. Lett. A **450**, 128365 (2022).
7. A. Fratalocchi, G. Assanto, K. A. Brzdakiewicz, *et al.*, Opt. Lett. **31**, 790 (2006).
8. M. Ezawa, Phys. Rev. B **99**, 201411 (2019).
9. H. Wang, K. Ji, Y. Wang, *et al.*, New J. Phys. **23**, 123039 (2021).
10. D. Leykam, M. C. Rechtsman, and Y. D. Chong, Phys. Rev. Lett. **117**, 013902 (2016).
11. L. C. Xie, H. C. Wu, X. Z. Zhang, *et al.*, Phys. Rev. B **104**, 125406 (2021).
12. Y. Wang, J. Yang, Y. Dang, *et al.*, Opt. Lett. **47**, 5437 (2022).
13. M. Z. Hasan and C. L. Kane, Rev. Mod. Phys. **82**, 3045 (2010).
14. B. Midya and L. Feng, Phys. Rev. A **98**, 043838 (2018).
15. M. G. Stojanović, S. Gündoğdu, D. Leykam, *et al.*, Phys. Scr. **97**, 030006 (2022).
16. I. Makasyuk, Z. Chen, and J. Yang, Phys. Rev. Lett. **96**, 223903 (2006).
17. T. C. V. Bzdušek and J. Maciejko, Phys. Rev. B **106**, 155146 (2022).
18. S. M. Zhang and L. Jin, Phys. Rev. A **100**, 043808 (2019).
19. R. G. Dias and A. M. Marques, Phys. Rev. B **105**, 035102 (2022).
20. B. Pal and K. Saha, Phys. Rev. B **97**, 195101 (2018).
21. M. G. Stojanović, M. S. Krasić, A. Maluckov, *et al.*, Phys. Rev. A **102**, 023532 (2020).
22. S. Flach, D. Leykam, J. D. Bodyfelt, *et al.*, Europhys. Lett. **105**, 30001 (2014).
23. R. A. Vicencio, C. Cantillano, L. Morales-Inostroza, *et al.*, Phys. Rev. Lett. **114**, 245503 (2015).
24. T. Bilitewski and R. Moessner, Phys. Rev. B **98**, 235109 (2018).
25. M. Kremer, I. Petrides, E. Meyer, *et al.*, Nat. Commun. **11**, 907 (2020).
26. V. I. Iglovikov, F. Hébert, B. Grémaud, *et al.*, Phys. Rev. B **90**, 094506 (2014).
27. B. Pal, Phys. Rev. B **98**, 245116 (2018).
28. T. Schwartz, G. Bartal, S. Fishman, *et al.*, Nature **446**, 52 (2007).
29. K. Ji, Z. Wen, Z. Liu, *et al.*, Opt. Lett. **43**, 4457 (2018).